



AMERICAN METEOROLOGICAL SOCIETY

Journal of Applied Meteorology and Climatology

EARLY ONLINE RELEASE

This is a preliminary PDF of the author-produced manuscript that has been peer-reviewed and accepted for publication. Since it is being posted so soon after acceptance, it has not yet been copyedited, formatted, or processed by AMS Publications. This preliminary version of the manuscript may be downloaded, distributed, and cited, but please be aware that there will be visual differences and possibly some content differences between this version and the final published version.

The DOI for this manuscript is doi: [10.1175/JAMC-D-13-0139.1](https://doi.org/10.1175/JAMC-D-13-0139.1)

The final published version of this manuscript will replace the preliminary version at the above DOI once it is available.

If you would like to cite this EOR in a separate work, please use the following full citation:

Sieglaff, J., L. Cronic, and W. Feltz, 2013: Improving satellite-based convective cloud growth monitoring with visible optical depth retrievals. *J. Appl. Meteor. Climatol.* doi:10.1175/JAMC-D-13-0139.1, in press.



1 **Improving satellite-based convective cloud growth monitoring with visible optical**
2 **depth retrievals**
3

4
5 Justin M. Sieglaff, Lee M. Counce, Wayne F. Feltz
6 *Cooperative Institute for Meteorological Satellite Studies, University of Wisconsin-*
7 *Madison, Madison Wisconsin*
8

9
10
11 *Corresponding author address:* Justin Sieglaff, 1225 West Dayton Street, Madison,
12 Wisconsin 53706. E-mail: justins@ssec.wisc.edu Telephone: 608.265.5357 Fax:
13 608.262.5974
14

15
16 Submitted to Journal of Applied Meteorology and Climatology on:
17 18 April 2013

18
19 Revisions Submitted:
20 18 July 2013

21
22 Re-Revisions Submitted:
23 20 September 2013
24
25

PRELIMINARY ACCEPTED VERSION

1 ABSTRACT

2 The use of geostationary satellites for monitoring the development of deep
3 convective clouds has been recently well documented. One such approach, the
4 University of Wisconsin Cloud-Top Cooling Rate (CTC) algorithm utilizes frequent
5 GOES observations to diagnose the vigor of developing convective clouds through
6 monitoring cooling rates of infrared window brightness temperature imagery. The CTC
7 algorithm was modified to include GOES visible optical depth retrievals for the purpose
8 of identifying growing convective clouds in regions of thin cirrus clouds.

9 An automated objective skill analysis of the two CTC versions (with and without
10 the GOES visible optical depth) versus a variety of NEXRAD fields was performed using
11 a cloud-object tracking system developed at UW-CIMSS. The skill analysis was
12 performed in a manner consistent with a recent study employing the same cloud-object
13 tracking system. The analysis indicates the inclusion of GOES visible optical depth
14 retrievals in the CTC algorithm increases probability of detection and critical success
15 index scores for all NEXRAD fields studied and slightly decreases false alarm ratios for
16 most NEXRAD thresholds. In addition to better identifying vertically growing storms in
17 regions of thin cirrus clouds, the analysis further demonstrates the strongest cooling rates
18 associated with developing convection are more reliably detected with inclusion of
19 visible optical depth, and storms that achieve intense reflectivity and large radar
20 estimated hail exhibit strong cloud top cooling rates in much higher proportions than
21 without inclusion of visible optical depth.

22

1 **1. Background**

2 The utility of geostationary satellite data for monitoring growing deep convective
3 clouds has been well documented in recent literature (Carvalho and Jones 2001; Morel et
4 al. 2002; Roberts and Rutledge 2003; Mecikalski and Bedka 2006; Vila et al. 2008;
5 Zinner et al. 2008; Sieglaff et al. 2011; Hartung et al. 2013). These studies have
6 demonstrated the key advantages of geostationary satellites for monitoring deep
7 convective cloud growth including frequent refresh rate (5-15 minutes), fine spatial
8 resolution (1-4 km), and expansive coverage (regional to full disk). Additionally, these
9 studies have demonstrated that satellite growth metrics (e.g., cooling infrared brightness
10 temperatures) often provide lead-time ahead of other remotely sensed convective
11 development metrics (e.g., exceedance of various radar reflectivity thresholds, detection
12 of storm electrification, etc.).

13 The University of Wisconsin Cloud Top Cooling Rate (CTC; Sieglaff et al. 2011)
14 algorithm was developed to quantitatively diagnose the vigor of vertical convective cloud
15 growth by determining cooling infrared window brightness temperatures (IRW BT)
16 between two consecutive GOES imager scans. The CTC output was recently related to
17 future Weather Surveillance Radar 1988-Doppler (WSR-88D) Next-Generation Radar
18 (NEXRAD 1985) observations in an automated objective manner, testing a hypothesis
19 that developing convective clouds with more intense vertical convective cloud growth
20 (inferred by stronger cloud top cooling) result in more intense precipitation signatures
21 observed by radar than comparatively weaker vertical convective cloud growth (Hartung
22 et al. 2013; H13 hereinafter). This hypothesis was confirmed; more intense CTC signals
23 resulted in higher radar reflectivity, larger Vertically Integrated Liquid (VIL; Greene and

1 Clark 1972), and larger Maximum Expected Size of Hail (MESH; Witt et al. 1998a) than
2 clouds with less intense CTC signals. These findings are consistent with previous studies
3 that related cooling rates of IRW BTs to environmental instability and associated updraft
4 /precipitation intensity (Adler and Fenn 1979a and 1979b, Alder et al. 1985, Roberts and
5 Rutledge 2003, Cintineo et al. 2013). Additionally, H13 showed the lead-time of CTC
6 signals to the occurrence of the variety of radar field thresholds studied. The lead-time
7 analysis showed the maximum CTC signal of a developing thunderstorm largely occurs
8 *prior* to the development of intense radar signatures. For example, the median lead-time
9 of maximum CTC signal to 0.25” and 1.00” MESH was 28 and 45 minutes, respectively.
10 This analysis showed the utility of the CTC algorithm to an operational forecaster, even
11 in regions well covered by radar.

12 The CTC output is generated in real-time at the University of Wisconsin and has
13 been transmitted to the National Oceanic and Atmospheric Administration (NOAA)
14 Hazardous Weather Testbed (HWT), University of Wisconsin Cooperative Institute for
15 Meteorological Satellite Studies (UW-CIMSS)/National Weather Service (NWS)
16 Milwaukee/Sullivan local HWT, and select NWS Weather Forecast Offices (WFOs)
17 since 2009. The feedback from NWS forecasters from the 2010 and 2011 testbeds (UW-
18 CIMSS 2013) were largely positive; however, the largest deficiency identified by the
19 2010-2011 testbed participants was the inability to diagnose cooling rates for storms
20 developing in areas of thin cirrus clouds. The CTC algorithm was originally designed to
21 not operate in areas of extensive ice clouds because cooling IRW BT between two GOES
22 imager scans, in the absence of other information, can be ambiguous. A cooling IRW BT
23 in a scenario with upper tropospheric cirrus clouds and lower tropospheric growing

1 cumulus clouds can be either of the following, or a combination of the two: 1) the upper
2 tropospheric cirrus clouds are growing thicker and hence absorbing more radiation from
3 the lower troposphere and emitting at the colder temperature of the cirrus clouds, or 2)
4 the lower cumulus clouds are growing vertically and hence are radiating at corresponding
5 colder temperatures as the cloud grows upward. Using an additional information source
6 from the GOES imager, the retrieved visible optical depth (Walther and Heidinger 2012),
7 can mitigate this ambiguity. In response to the forecaster feedback, the CTC algorithm
8 was improved during early 2012 to address this shortcoming by incorporating the GOES
9 visible optical depth (τ_{vis}) retrievals. The new version of the algorithm was supplied to
10 the NOAA HWT and local NWS WFOs beginning in April 2012 (GOES-R Proving
11 Ground 2013).

12 The goals of this manuscript are 1) to document the inclusion of τ_{vis} into the CTC
13 algorithm and 2) provide a reader/forecaster a measure of increased CTC algorithm skill
14 by including τ_{vis} . This paper is presented as follows: Section 2 describes the data and
15 methodology used to improve the CTC algorithm. Additionally, some examples are
16 provided to illustrate the improvement of the CTC output by including τ_{vis} . Section 3
17 provides a statistical analysis of the improved CTC output (CTCv2 or “v2”) versus CTC
18 output without τ_{vis} (CTCv1 or “v1”) in a manner consistent with H13. Section 4
19 summarizes key findings and provides information for accessing the experimental real-
20 time feed of v2 algorithm output.

21

22 **2. Data and Methodology**

23 *a. Data*

1 *GOES-12* imager data over the Continental United States (CONUS) is used for 23
2 convectively active afternoons over the Central Plains during the spring and early
3 summer of 2008 and 2009. The validation domain is consistent with Sieglaff et al.
4 (2011) and H13 (Central and Southern Plains; bounded by 30°N to 46°N and from 94°W
5 to 104°W) and includes regions of both expected severe thunderstorms and non-severe
6 thunderstorms—which encompasses convectively active regions with low instability,
7 high instability/high vertical wind shear, and high instability/low vertical wind shear.
8 Possible future work may increase the domain size, allowing for increased sample sizes
9 and for grouping the analysis based upon instability/wind shear combinations. All
10 *GOES-12* data are at the 4 km nadir IR resolution, including visible data (largely for
11 computational efficiency and ease of processing). The *GOES-12* imager data is used in
12 many ways; 1) as input into a cloud object tracking system, 2) input into GOES cloud
13 mask (Heidinger 2010), cloud phase (Pavolonis 2010), and cloud optical depth retrieval
14 algorithms (Walther and Heidinger 2012), and 3) input into the CTC algorithm. Quality-
15 controlled NEXRAD 0.01 degree WSR-88D radar data were provided by the Cooperative
16 Institute for Mesoscale Meteorological Studies at the University of Oklahoma (OU-
17 CIMMS) (Lakshmanan et al. 2007). The radar fields used in this study include
18 reflectivity at the -10°C isotherm (Ref.₁₀; Lakshmanan et al. 2006), VIL, and MESH and
19 are used in the analysis section where CTC output is related these fields.

20

21 *b. Methodology Background*

22 The CTC algorithm uses two consecutive GOES imager scans to compute a ‘box-
23 averaged’ IRW BT cooling rate leveraging GOES Cloud Mask (Heidinger 2010) and

1 GOES Cloud Phase (Pavolonis 2010) algorithms to identify cloudy satellite pixels and
2 classify the phase (water, supercooled water, mixed, and ice phases) of the clouds,
3 respectively. The CTC methodology utilizes a two-box system, a small box (7x7 satellite
4 pixels) to compute the average IRW BT for cloudy pixels and a large box (13x13 satellite
5 pixels) to compute a variety of metrics. The large box metrics are used in a series of tests
6 to identify areas of cooling IRW BTs attributed to vertically growing clouds and
7 eliminate ‘false’ cooling due to horizontal cloud advection. A high-level summary of
8 CTC processing is: 1) computation of box-averaged IRW BTs, 2) temporal differencing
9 of box-averaged IRW BTs to produce unfiltered cloud top cooling rates, 3) apply series
10 of tests filtering false cooling rates due to horizontal cloud advection and other undesired
11 artifacts with end product being the final filtered CTC field. Full details of the CTC
12 algorithm are not included here; the reader is encouraged to reference Sieglaff et al.
13 (2011) for complete algorithm detail. The brief summary given is intended to provide
14 sufficient background for understanding the description of incorporating τ_{vis} into the CTC
15 algorithm.

16 The GOES visible optical depth (Walther and Heidinger 2012) is a dimensionless
17 quantity representing the extinction of radiation between the satellite and the Earth’s
18 surface (Nakajim and King 1990; Platnick, et al. 2003). A cloud-free atmosphere will
19 have τ_{vis} near zero (not absolutely zero due to trivial gaseous extinction), to small values
20 (up to ~ 10) for cirrus clouds, and in the ~ 10 s to ~ 100 for deep cumuliform clouds
21 (Platnick et al. 2003). As such, significant separation exists between cumuliform clouds
22 and thin cirrus clouds in the retrieved visible optical depth fields. This separation is
23 exploited when incorporating τ_{vis} into v2. Mecikalski et al. (2011) showed the τ_{vis} of

1 immature, yet vertically growing cumulus clouds reaches a median value of
2 approximately 25, with considerable spread to larger values (larger interquartile value of
3 approximately 75) 0-45 minutes prior to 35 dBZ rainfall reaching the surface, further
4 motivating the use of optical depth in diagnosing convective development. Figure 1
5 illustrates T_{vis} retrievals with more familiar GOES visible and IRW BT imagery (all fields
6 at 4 km GOES resolution) for developing thunderstorms over eastern IL/western IN valid
7 1910-1932 UTC 30 March 2012. It is clear from the visible and IRW imagery (Fig. 1)
8 convective clouds are growing vertically and horizontally and becoming colder. The
9 corresponding T_{vis} retrievals in this line of developing convection are also increasing with
10 time. It is the co-location of cooling IRW BTs and increasing T_{vis} retrievals that are
11 exploited to diagnose cloud-top cooling in regions of thin cirrus clouds. The CTC
12 algorithm ‘ice mask’ (Fig. 1, defined below) indicates a large area of thin cirrus clouds
13 that largely prevented v1 from diagnosing the cloud-top cooling rates with these storms
14 (a comparison between v1 and v2 for this case is shown in Figure 2). The T_{vis}
15 improvement is used only for solar zenith angles of 70 degrees and less; in regions with
16 solar zenith angles greater than 70 degrees, the v1 logic fully applies with no attempt to
17 include T_{vis} information.

18 As mentioned previously, the v1 algorithm was designed to not operate in areas of
19 ice clouds due to potential ambiguity associated with cooling IRW BTs in these regions.
20 Specifically the v1 algorithm omits any cooling rates for a pixel in which the large box
21 contains 50% or greater ice cloud fraction (Sieglaff et al. 2011). This ice fraction test
22 omits developing storms beneath thin cirrus clouds and in some cases the strongest cloud
23 top cooling rates with developing storms when the strongest cooling occurs after the

1 developing storm top had sufficiently glaciated. T_{vis} has been incorporated into the CTC
2 algorithm and acts as a restoral, meaning the v1 algorithm flow is maintained and the T_{vis}
3 logic described in this section only acts to add cloud-top cooling rates to the final output
4 field. As such, subsequent skill analysis and comparisons between v2 and v1 are for
5 daytime only (when T_{vis} retrievals are available). The v2 skill scores are only valid for
6 daytime, while the v1 skill scores as well as the results of H13 apply for night-time
7 scenes (when T_{vis} is unavailable).

8

9 *c. Incorporating T_{vis} into CTC algorithm*

10 The v1 algorithm utilizes seven tests to remove false cooling rates and these tests
11 are broken into two groups; two major tests that screen out false cooling rates due to
12 horizontal cloud advection and five minor tests to screen out further false cooling
13 rates/undesirable scenarios, such as the ice cloud percentage test mentioned previously.
14 T_{vis} is integrated into the CTC algorithm by applying the two major tests to the unfiltered
15 cloud-top cooling rate field to produce an intermediate, partially filtered cloud-top
16 cooling rate field. One additional minor test is applied to this partially filtered cloud-top
17 cooling rate field and screens the cooling rates for clouds determined to be marginally
18 cooling. This minor test can remove vertically growing pixels at the very early stages of
19 growth, but not all cooling clouds within the very early stages of growth will mature into
20 thunderstorms. This test acts to reduce false alarms (Sieglaff et al. 2011). After these
21 three filtering steps are complete, these remaining cloud-top cooling rates are candidates
22 for being restored into the final v2 output field pending the methodology described
23 below.

1 The \mathbf{T}_{vis} field for both (current and previous) satellite scans is box-averaged using
2 the small box previously described. The partially filtered candidate cloud-top cooling
3 rate pixels are tested for specific conditions related to the \mathbf{T}_{vis} fields. For a pixel to be
4 restored from the partially filtered cloud-top cooling rate field into the final v2 output, the
5 following conditions must be met: 1) The box-averaged \mathbf{T}_{vis} time rate of change must be
6 positive ($> 1.0 (15 \text{ min})^{-1}$), and 2) the maximum box-averaged \mathbf{T}_{vis} within the small box at
7 the current time must be sufficiently large (> 25.0). The positive temporal trend of \mathbf{T}_{vis} is
8 straightforward; it should be increasing for vertically growing and horizontally expanding
9 convective cloud. The sufficiently large threshold of 25.0 was chosen based upon
10 Mecikalski et al. (2011). When these conditions within the \mathbf{T}_{vis} fields are met, the
11 partially filtered cloud-top cooling rate is restored into the final v2 output field. Figures 2
12 and 3 illustrate the improvement of the v2 versus v1. The case shown in Fig. 2 is the
13 same date, time, and location as Fig. 1; note how v1 only detects cloud-top cooling rates
14 on one developing storm at 1915 and 1925 UTC just east of the IL/IN border. V2
15 identifies four additional storms in regions identified as ice cloud covered (one in eastern
16 IL and three additional storms in IN; Fig. 2). Fig. 3 is another example of improved
17 cloud-top cooling rate detection with v2 for a case of dry-line convection in Oklahoma on
18 14 April 2011. Thin cirrus clouds covered much of Oklahoma at this time (see CTC ice
19 mask; Fig. 3); as such v1 only detected two storms near the Red River at 1940-1955 UTC
20 and 2010 UTC (absence of thin cirrus). The v2 algorithm detected three additional
21 storms over northern OK between 1955 and 2010 UTC (Fig. 3) as well as the most
22 intense period of cooling of the storm just north of the Red River (2003 UTC), which was
23 missed by v1. These examples demonstrate the improvement of specific cases; the

1 improvement in the form of bulk statistics, over the 23 days studied are presented in the
2 following section.

3

4 **3. Analysis**

5 *a. Background and Previous Studies*

6 Previous work performed by H13 demonstrated the relationships between v1
7 output and future NEXRAD observations for developing thunderstorms. H13 used an
8 automated cloud object tracking system that creates cloud objects from GOES imager
9 observations, assigns each object an unique ID, and tracks these objects through space
10 and time, all while maintaining the unique ID (Sieglaff et al. 2013). The cloud-object
11 tracking system utilizes the Warning Decision Support System - Integrated Information
12 (WDSS-II; Lakshmanan et al. 2007) framework developed at the University of Oklahoma
13 to group adjacent cloudy satellite pixels into cloud-objects, similar to how a human
14 would analyze satellite or radar data, and track these cloud-objects through space and
15 time. A post-processing utility then merges the WDSS-II output and performs steps to
16 minimize the broken tracks of convective cloud-objects. The cloud-object tracking
17 system is designed to track convective clouds from infancy *into* the mature phase and
18 provide a means to generate statistics of any number of meteorological fields, as well as
19 temporal trends of such fields for each cloud-object within a time period of interest. The
20 object tracking system supports various geo-spatial data including satellite observations,
21 satellite algorithm output (such as CTC output), NEXRAD observations and derived
22 fields, and numerical weather prediction (NWP) data, etc. The object tracking system
23 allows for an objective, automated methodology to validate and determine relationships

1 between each developing convective cloud's cloud-top cooling rate and future NEXRAD
2 observations, as well as the lead-time the CTC signals provide ahead of NEXRAD
3 observations. The details of the convective cloud-object tracking system are out of the
4 scope of this article; full details can be found in Sieglaff et al. (2013).

5 The analysis presented in this section utilizes the identical framework as that
6 described by H13 and Sieglaff et al. (2013). Consistent with H13, these comparisons do
7 not include comparisons to surface storm reports or severe thunderstorm warnings.
8 While these comparisons would be useful, and are the goals of future work, NEXRAD
9 data and derived output (e.g., MESH) are the focus of this study. Many studies have
10 documented the limitations of storm report data (Witt et al. 1998b; Stumpf et al. 2004;
11 Ortega et al. 2006). Cintineo et al. (2012) demonstrated that multi-radar MESH provides
12 superior coverage and spatial resolution over storm reports, is free from non-
13 meteorological biases, and is a good discriminator for the severe-sized hail threshold
14 (1.00"). This enables direct comparisons between v1 and v2 for the identical population
15 of cases.

16 Since v2 is only different from v1 during the daytime (specifically solar zenith
17 angles less than 70 degrees), the comparisons between v1 and v2 are not directly drawn
18 from H13 because that study combined daytime and nighttime scenes. As such, the
19 comparisons between the two CTC versions are for 23 convectively active afternoons
20 (1800 – 0000 UTC) over the Central Plains of the United States during the spring and
21 early summer of 2008 and 2009. The total number of cloud objects considered in the
22 validation with valid Ref₁₀ is 3,153 and the breakdowns as a function for multiple
23 NEXRAD fields/thresholds are provided in Table 1. The statistical analysis and

1 comparisons presented herein are intended to demonstrate the improved algorithm skill
2 by incorporating \mathbf{T}_{vis} into the CTC algorithm. Similarities and differences of
3 relationships between versions of CTC with NEXRAD observations are also presented.

4 Consistent with H13, CTC [K (15 min)^{-1}] data points are grouped into three bins
5 (weak: $\text{CTC} > -10$; moderate: $-10 \geq \text{CTC} > -20$; strong: $\text{CTC} \leq -20$), however only CTC
6 signals that precede or occur concurrently to the occurrence of a given NEXRAD
7 threshold are counted as hits (e.g., lead-times less than 0 min are counted as misses),
8 while H13 counted CTC signals with lead-time of -17 min and greater as hits; therefore,
9 comparisons between this study and H13 need to account for this difference..

10

11 *b. Caveats applicable to statistical analysis*

12 The subsequent section presents a skill analysis for the two versions of CTC
13 versus three NEXRAD fields; however, a discussion related to the limitations of the
14 automated objective validation technique and how to interpret the resultant statistics is
15 first necessary. The automated cloud object tracking system (used by H13 and herein)
16 was designed to track growing convective clouds from infancy *into* satellite maturity
17 (presence of thunderstorm anvils). Ultimately thunderstorm anvils merge together and
18 tracking of separate thunderstorms becomes difficult, if not impossible, only using
19 satellite data. While efforts were made to track storms as long as possible, tracking of
20 any specific storm could end prior to achieving maximum intensity as defined by a
21 variety of NEXRAD metrics (H13; Sieglaff et al. 2013). This has a direct impact on the
22 statistical analysis of probability of detection (POD), false alarm ratio (FAR), and critical
23 success index (CSI). Specifically, there is an underrepresentation of extreme NEXRAD

1 values (intense reflectivity, large estimated hail size, etc.) in the validation framework.
2 *As such, for increasing NEXRAD intensity, the POD values are likely underestimates and*
3 *the FAR values are likely overestimates (HI3) thereby leading the CSI scores to be*
4 *underestimates.* Consider the following example: A developing storm with valid CTC
5 signal is tracked successfully to a point of reaching 55 dBZ reflectivity, 0.25" MESH,
6 and 30 kg m⁻² VIL; thereafter the storm is no longer tracked since it merged into a large
7 anvil mass. For NEXRAD fields greater than these values, that cloud-top cooling rate is
8 counted as a false alarm. Additionally, the number of hits at extreme values is also
9 decreased, which since such a storm had a valid cloud-top cooling rate, the POD and CSI
10 scores are likewise decreased. As a final point, the validation domain is expansive and
11 not limited to only regions of expected severe weather, so a proportion of the storms in
12 the analysis should not be expected to reach intense/severe NEXRAD values. As such
13 the expanse of the validation domain acts to decrease POD/CSI for these intense/severe
14 NEXRAD values than if one only considers regions supportive for severe thunderstorms.
15 While these caveats are imperative to consider when assessing the specific performance
16 scores, the statistical differences between the two CTC algorithms are impacted
17 identically, so relative changes can be attributed solely to algorithm modifications and
18 not to any validation framework shortcomings.

19

20 *c. NEXRAD derived skill analysis*

21 *i. Reflectivity at -10°C*

22 Table 1 shows hits, misses, false alarms, POD, FAR, and CSI for v2 (bold) and v1
23 for Ref.₁₀. Table 2 shows the *total number of cloud objects* having a valid NEXRAD

1 signal and valid cloud-top cooling rate broken down by cooling rate strength, and these
2 totals are only for the *maximum* cloud-top cooling rate observed in a cloud object lifetime
3 (valid means there were non-missing NEXRAD and CTC values for a given cloud
4 object). As such, these totals equal the hits in Table 1 for the two CTC versions. Table 3
5 shows the *total instances* of cloud objects having a valid NEXRAD signal and valid CTC
6 signal for each CTC strength bin (a single cloud object could potentially be counted in
7 each CTC bin). For example, a storm may initially have a weak CTC signal, the
8 following scan have a moderate CTC signal, and later exhibit a strong CTC signal;
9 therefore, Table 3 has a larger population than Table 2.

10 The v2 exhibits an increase of hits (and decrease of misses) for all Ref.₁₀ bins
11 (Table 1). The POD for strong to intense Ref.₁₀ (50 dBZ and larger) increases for v2
12 versus v1 with a general rise of 0.06 to 0.13 (from 0.38-0.58 to 0.44-0.71). Further
13 examination of POD metrics indicate the majority of storms achieving strong to intense
14 Ref.₁₀ exhibited strong cloud-top cooling rates in v2 and at a much higher proportion than
15 that of v1. The increased proportion of strong CTC values for v2 is due to increased data
16 points added by the **T_{vis}** algorithm methodology. In v1, the ice cloud percentage test
17 often prevented the strongest cooling rate from being diagnosed; in some cases only the
18 initial cooling rate was diagnosed (belonging to weak or moderate bins). The inclusion
19 of the **T_{vis}** trend and magnitude into the v2 algorithm allows for more successful
20 identification of the strongest cooling rate (note the much larger fraction of strong
21 cooling rates for v2 than v1 in Table 2, in addition to more storms being diagnosed).
22 Despite a small increase in the total number of false alarms in v2 than v1, the FAR

1 increases only slightly for Ref.₁₀ 45 dBZ and less and remains unchanged or slightly
2 decreases for Ref.₁₀ 50 dBZ and larger (Table 1).

3 The increased POD and decreased FAR for Ref.₁₀ translate into slightly increased
4 CSI scores for v2 over v1 (Table 1) when assessing total CSI, but when considering only
5 the strong CTC hits, the CSI scores increase by larger proportions, especially for
6 strong/intense Ref.₁₀. The largest CSI value for all CTC occurs at 50 dBZ (0.27 v2; 0.23
7 v1) and at 55 dBZ when considering only the strong CTC (0.32 v2; 0.22 v1). The
8 implication of maximum CTC skill for storms achieving 50 or 55 dBZ at Ref.₁₀ should be
9 taken with caution, however. Recall the previous discussion related to cloud object
10 tracking limitations. While not every storm that achieves 50 dBZ will go on to reach 55
11 or 60 dBZ, the cloud object tracking limitations compound the decrease in number of
12 storms reaching more intense values. To definitively declare the CTC algorithm to be
13 most skillful for a specific reflectivity threshold should be made with caution, but the
14 relative increase in skill between v2 and v1 is unaffected by these concerns.

15 In general, v2 exhibits more skill in identifying storms for all values of Ref.₁₀ than
16 v1 with the most notable increase for moderate/strong Ref.₁₀. The v2 (compared to v1)
17 algorithm identifies more storms with a POD as high as 0.71 (0.58) for 60 dBZ Ref.₁₀.
18 Additionally, the increased identification of the strongest cooling rates (and associated
19 large percentage of strong Ref.₁₀ values) by v2 can lend to increased confidence that a
20 developing storm should exhibit strong CTC signal if strong Ref.₁₀ is to be achieved later
21 in the storm lifecycle than one would expect with v1.

22

23 *ii. Maximum Expected Size of Hail (MESH)*

1 Table 4 shows hits, misses, false alarms, POD, FAR, and CSI for v2 (bold) and v1
2 for MESH. Similar to Ref.₁₀, the number of hits increased (and misses decreased) for all
3 values of MESH. The POD significantly improves by 0.15-0.20 for all total MESH bins.
4 V2 captures 64% of all storms generating any hail (0.25+” MESH) and 83% of storms
5 with radar estimated severe hail (1.00+”) while v1 only achieved 51% and 67% for these
6 MESH thresholds. The majority of all storms producing any hail (0.25+” MESH) exhibit
7 strong v2 and effectively every storm exhibiting radar estimated severe hail (1.00+”
8 MESH) had moderate or strong cloud-top cooling rates in v2; much less of a definite
9 relationship is observed with v1. The proportion of storms reaching the strong CTC bin
10 is again much higher for v2 than v1 due to **T_{vis}** enabling detection of each storm’s
11 strongest cooling rate (Tables 2 and 4). The FAR values are generally slightly smaller for
12 v2 than v1 when considering all CTC data points. This translates into increased CSI
13 scores for v2 relative to v1. The CSI scores for the total CTC bins generally increase
14 slightly for v2 compared to v1, but when only considering the strongest CTC bin, the
15 skill increases by as much as ~0.15.

16 Like with Ref.₁₀, the apparent decrease in skill for increasing MESH needs to be
17 taken in context. The validation domain contains storms within regions where severe
18 convection was not expected and the limitations of the cloud object tracking system
19 contribute to fewer storms reaching severe hail sizes than actually occur. Perhaps the
20 most useful skill metric is the v2 POD numbers (0.83 for 1.00+” MESH, 0.91 for 1.50+”
21 MESH). These extremely high POD numbers suggest when the environment is
22 supportive for severe hail, a forecaster can have very high confidence the v2 algorithm
23 will identify a storm that will achieve radar estimated severe hail and likely have a strong

1 CTC (Table 4). While the FAR values are quite high, this is expected because severe hail
2 is quite rare relative to all thunderstorms (consider count decreases from Ref.₁₀ to MESH
3 in Table 2 and the prior statement that valid cloud-top cooling rates with no associated
4 NEXRAD bin value are counted as false alarms). Also, the FAR values, while high, are
5 slightly lower than the POD numbers for v2.

6 Overall v2 is shown to be more skillful in diagnosing storms that produce any
7 radar estimated hail (0.25+” MESH), with high POD for storms producing severe MESH.
8 Of most significance is the very large proportion of storms that produce radar estimated
9 hail exhibit strong CTC. Again, this suggests to a forecaster that in an environment
10 supportive of hail development, any developing storm that will produce hail, particularly
11 severe hail, should be expected to exhibit strong CTC, especially with v2.

12

13 *iii. Vertically Integrated Liquid (VIL)*

14 Table 5 shows hits, misses, false alarms, POD, FAR, and CSI for v2 (bold) and v1
15 for VIL. The various skill metrics for VIL exhibit very similar improvements as Ref.₁₀
16 and MESH. For brevity an in depth analysis of VIL is omitted, but Table 5 shows the full
17 statistics. The most important points are that, in general, the POD numbers are again
18 improved for all VIL thresholds for v2 compared to v1 with very high POD (> 0.80) for
19 VIL of 40 kg m⁻² and larger. The largest CSI scores are associated with strong CTC
20 values, suggesting a forecaster should expect strong CTC values (especially v2) with any
21 developing storm in regions where large VIL are anticipated.

22

23 *d. CTC and maximum NEXRAD distributions*

1 Using the hits from Tables 1, 4, and 5, distributions of maximum radar value
2 achieved (for Ref.₁₀, MESH, and VIL) versus all CTC and maximum CTC were
3 constructed. Figures 4-6 show distributions of all and maximum CTC versus maximum
4 NEXRAD value achieved for Ref.₁₀, MESH, and VIL, respectively. In Figures 4-6, the
5 left panels are for v2 and the right panels are for v1; the top panels correspond to all CTC
6 (any storm may have more than one valid cloud-top cooling rate diagnosed) and the
7 bottom panels correspond to a cloud object's maximum cloud-top cooling rate observed.

8 The distributions in Fig. 4a,c show generally wide distributions for all CTC versus
9 maximum Ref.₁₀ for each CTC bin. The weak and moderate CTC bins do not show any
10 appreciable differences between the two algorithm versions; however, the strong bin for
11 v2 (Fig. 4a) has a significantly more narrow distribution (bottom 1σ value is 40 dBZ
12 instead of 30 dBZ and the 25th percentile value is 45 dBZ instead of 40 dBZ) and a larger
13 median Ref.₁₀ of 55 dBZ instead of 50 dBZ. The narrower distribution width and larger
14 median suggest the added strong CTC points of v2 are more often associated with storms
15 that achieve more intense Ref.₁₀, which agrees with the skill score analysis. Figures 4b,d
16 are the same as Figs. 4a,c except only the maximum CTC for a cloud object is
17 considered. The distributions in Fig. 4b,d are significantly narrower compared to all CTC
18 (Fig. 4a,c), simply because the initial weaker growth of strong storms are omitted in the
19 maximum CTC distributions (included in the all CTC distributions). The v2 distributions
20 (Fig. 4b) are generally narrower (toward larger (smaller) Ref.₁₀ for the strong (weak)
21 CTC bin) than those for v1 (Fig. 4d). The narrowing and shift toward smaller Ref.₁₀ for
22 the weak CTC is attributed to the increased diagnosis of strong cooling rates with v2.
23 The better diagnosis of strong cooling rates, in turn, results in the weak CTC bin to be

1 populated with storms that never actually achieve moderate or strong cooling rates as
2 opposed to storms that did have strong growth but the strong growth period was missed
3 in v1. The narrowing and shift toward larger Ref.₁₀ for the strong CTC occurs for similar
4 reasons; the added data points are largely from storms that achieve strong to intense Ref.
5 ₁₀ (Table 2: 109 strong v2; 63 strong v1). These distributions give increased confidence
6 that a strong cooling rate from v2 will result in strong to intense Ref.₁₀ and that a
7 developing storm with only weak cooling in v2 will, in general, not develop strong to
8 intense Ref.₁₀ when compared to v1.

9 Figure 5 is the same as Figure 4, except for MESH. Similar relationships exist
10 between all CTC and maximum MESH (Fig. 5a,c) as shown with Ref.₁₀. The v2
11 distributions for weak and moderate are more constrained to smaller MESH values than
12 v1, while the strong CTC bin is largely the same. When considering the maximum CTC
13 (Fig. 5b,d), the distributions are again much narrower for v2 than v1 for similar reasons
14 to those with Ref.₁₀. (The weak bin in Fig. 5b is very narrow, largely due to a very small
15 sample size (6 storms had a maximum v2 in the weak bin and 0.25+” MESH).) When
16 considering maximum CTC, v2 (Fig. 5b) has much narrower distributions shifted to
17 smaller MESH values in the weak and moderate bins than v1 (Fig. 5d), as well as smaller
18 populations (Table 2). The strong bin is largely the same between the two CTC versions.
19 Figures 5b,d imply that one can more confidently expect radar estimated severe hail
20 (1.00+”) when a developing storm exhibits strong cloud-top cooling rates in v2 than was
21 possible with v1 (where severe hail was more common in the weak and moderate CTC
22 bins).

1 Figure 6 is the same as Figs. 4 and 5, except for VIL. Again, for brevity, a full
2 analysis of Fig. 6 is omitted. The key points taken from Fig. 6 are similar to those of
3 Figs. 4 and 5; a forecaster can have increased confidence that a developing storm with
4 strong (weak) v_2 will more likely produce large (small) VIL values in the future than
5 could be deduced from the analysis of v_1 .

6 H13 included a lead-time analysis of CTC signal (both all and maximum) ahead
7 of maximum NEXRAD values obtained for each storm, as well as lead-time ahead of
8 operationally significant thresholds (e.g., MESH 1.00" and VIL 40 kg m⁻²). The lead-
9 times from H13 indicate 20 (60+) minute lead-time for VIL values of 20 (45) kg m⁻² and
10 45 minute lead-time for severe hail MESH (1.00"). While the lead-time threshold that
11 defines hits differs between H13 and this manuscript (-17 min and 0 min, respectively),
12 the lead-times determined herein were very similar to those reported by H13. As such
13 only median lead-time for v_2 and v_1 for various thresholds of Ref.₁₀, MESH, and VIL are
14 provided in Table 6. The most significant difference between the CTC versions was
15 toward smaller median lead-times from v_2 compared to v_1 for the 23 days studied. This
16 trend is not unexpected given the added v_2 data points are a result of including T_{vis}
17 trends, which occur at a slightly later stage in storm development and that the strongest
18 cooling rates are more reliably detected (occur later than preceding weaker CTC). The
19 slight decrease in lead-time does not limit the usefulness of v_2 data as demonstrated at
20 the 2012-3 NOAA HWT (GOES-R Proving Ground 2013), especially given the increased
21 algorithm skill for operationally significant echoes.

22

23 **4. Summary**

1 The use of high spatial and high temporal resolution remote sensing data is
2 essential when monitoring the development and growth of deep convective storms. The
3 University of Wisconsin-Cloud Top Cooling Rate (CTC) algorithm was developed to
4 monitor the vertical growth rate of developing convective clouds by diagnosing regions
5 of cooling IRW BTs between consecutive GOES imager scans. Feedback from various
6 experiments with operational meteorologists indicated the largest deficiency of the v1
7 was the inability to diagnose cooling rates in regions of thin cirrus clouds. The v1
8 algorithm was designed to exclude regions dominated by cirrus clouds because cooling
9 IRW BTs in regions of cumulus cloud growth shielded by upper level cirrus clouds can
10 be ambiguous in the absence of additional information. To address this deficiency, the
11 CTC algorithm was modified to include τ_{vis} retrievals. The inclusion of τ_{vis} retrievals
12 (v2) increased the identification of developing storms that were otherwise missed by v1.

13 A skill score analysis compared the output of v1 and v2 against many NEXRAD
14 fields and thresholds (Ref.₁₀, MESH, and VIL) for 23 convectively active days from
15 spring/early summer 2008 and 2009. It is important to reiterate the skill analysis of v2
16 applies to daytime—when visible optical depth retrievals are available. Near the
17 terminator and at night the v1 logic applies and the v1 skill scores and results from H13
18 best describe the algorithm performance in those conditions. The skill score analysis
19 shows the inclusion of τ_{vis} into the CTC algorithm acts to increase POD for all thresholds
20 of all NEXRAD fields analyzed, especially for strong/intense values of those fields (e.g.,
21 POD for 50, 55, and 60 dBZ Ref.₁₀ for v2 (v1): 0.44 (0.38), 0.57 (0.48), and 0.71 (0.58),
22 respectively). The CSI was shown to slightly increase for most thresholds of the
23 NEXRAD fields for v2 relative to v1, with more notable CSI increases for strong CTC

1 and strong/intense Ref.₁₀, MESH, and VIL. The analysis also demonstrated that v2 more
2 often identified the strongest vertical growth rate (cooling rate), whereas v1 sometimes
3 missed the strongest cloud-top cooling rate due to specific algorithm configuration (e.g.,
4 ice cloud percentage test). The more complete identification of the strongest cloud-top
5 cooling rates with v2 acted to narrow the distributions of maximum CTC and maximum
6 NEXRAD values and shift those distributions to more intense (weak) NEXRAD values
7 for strong (weak) CTC bins compared to v1 (even in regions absent of thin cirrus
8 shields). In practical terms, a forecaster can have increased confidence in the following:
9 1) developing storms with strong CTC values will more often be associated with future
10 strong/intense NEXRAD observations and storms with weak CTC values will more often
11 fail to reach strong/intense NEXRAD values, 2) the strongest cloud-top cooling rate of a
12 developing storm will more often be successfully identified, 3) growing cumulus clouds
13 within regions of thin cirrus clouds will more often be detected, and 4) developing storms
14 that will achieve severe radar estimated hail (1.00+” MESH), strong Ref.₁₀ (55+ dBZ),
15 and large VIL (30+ kg m⁻²) will most often exhibit strong CTC with v2 than v1.
16 Additionally, the inclusion of **T_{vis}** results in only a small reduction of lead-time of the
17 maximum CTC signal to NEXRAD observed reflectivity and derived field thresholds.
18 Finally, it is important that the relatively high FAR for intense Ref.₁₀, radar estimated
19 severe hail (via MESH), etc. are taken in context. The high FAR values are due to: 1)
20 the validation domain encompassed regions of expected severe and non-severe
21 thunderstorms, 2) intense reflectivity, large hail, etc., being rare relative to all
22 thunderstorms, and 3) the satellite-based cloud tracking validation technique employed
23 being designed to track *into* the mature thunderstorm stage, and not necessarily to radar

1 maturity. Therefore, the database is, to a degree, an underrepresentation of maximum
2 NEXRAD intensity actually achieved. However, given the high POD values of v2 for
3 intense radar signatures [e.g., 0.83 for 1.00+” MESH, 0.71 for 60 dBZ Ref.₁₀], when
4 considering the mesoscale and synoptic environmental conditions, in situations favorable
5 for severe weather, a developing storm will likely exhibit strong CTC prior to the onset of
6 intense reflectivity and/or large radar estimated hail in most cases.

7 The v2 output has been generated in real-time at UW-CIMSS since April 2012
8 and is available currently via the CIMSS local data manager. For more details on how to
9 ingest CTC fields into AWIPS see ([http://cimss.ssec.wisc.edu/goes_r/proving-](http://cimss.ssec.wisc.edu/goes_r/proving-ground/awips/ci/index.html)
10 [ground/awips/ci/index.html](http://cimss.ssec.wisc.edu/goes_r/proving-ground/awips/ci/index.html)) and for quicklook imagery on the web see
11 (<http://cimss.ssec.wisc.edu/snaap/convinit/quicklooks/>).

12

13 **5. Acknowledgements**

14 We are thankful for the opportunity to perform this work under the NOAA GOES
15 Product Assurance Plan (GIMPAP) program, federal grant number NA10NES4400013.
16 We would like to thank the many NWS forecasters that have used CTC data and provided
17 valuable feedback for improving the algorithm. We are also grateful for the expertise and
18 openness of the GOES-R Cloud Team at NOAA/STAR and UW-CIMSS in incorporating
19 various cloud retrievals into the CTC algorithm.

20

21

Appendix

22

List of Acronyms

T_{vis}	Visible optical depth
BTs	Brightness Temperatures

CSI	Critical Success Index
CTC	Cloud-Top Cooling
dBZ	Decibels relative to Z
FAR	False Alarm Ratio
GOES	Geostationary Operational Environmental Satellite
HWT	Hazardous Weather Testbed
IRW	Infrared Window
MESH	Maximum Expected Size of Hail
NEXRAD	Next Generation Radar
NOAA	National Oceanic and Atmospheric Administration
NWS	National Weather Service
POD	Probability of Detection
Ref. ₁₀	Reflectivity at -10°C isotherm
UW-CIMSS	University of Wisconsin – Cooperative Institute for Meteorological Satellite Studies
v1	Version 1 of CTC algorithm
v2	Version 2 of CTC algorithm
VIL	Vertically Integrated Liquid
WDSS-II	Warning Decisions Support System – Integrated Information
WFO	Weather Forecast Office
WSR-88D	Weather Surveillance Radar – 88 Doppler

1

2

3 **6. References**

4 Adler, R. F., D. D. Fenn, 1979a: Detecting Severe Thunderstorms using Short-Interval

5 Geosynchronous Satellite Data. *Bull. Am. Meteorol. Soc.*, **60**.

6 Adler, R. F., D. D. Fenn, 1979b: Thunderstorm Intensity as Determined from Satellite

7 Data. *J. Appl. Meteorol.*, **18**, doi:10.1175/1520-

8 0450(1979)018<0502:TIADFS>2.0.CO;2.

9 Adler, R. F., M. J. Markus, and D. D. Fenn, 1985: Detection of Severe Midwest

10 Thunderstorms using Geosynchronous Satellite Data. *Mon. Weather Rev.*, **113**,

11 doi:10.1175/1520-0493(1985)113<0769:DOSMTU>2.0.CO;2.

1 Carvalho, L. M. V., and C. Jones, 2001: A satellite method to identify structural
2 properties of mesoscale convective systems based on the Maximum Spatial
3 Correlation Tracking Technique (MASCOTTE). *J. Appl. Meteor.*, **40**, 1683-1701.

4 Cintineo, J. L., M.J. Pavolonis, J.M. Sieglaff, and A.K. Heidinger, 2013: Evolution of
5 Severe and Non-severe Convection Inferred from GOES-derived Cloud
6 Properties. *J. Appl. Meteor.*, Accepted.

7 Cintineo, J. L., T. M. Smith, V. Lakshmanan, H. E. Brooks, and K. L. Ortega, 2012: An
8 Objective High-Resolution Hail Climatology of the Contiguous United States.
9 *Wea. Forecasting*, **27**, 1235-1235-1248.

10 GOES-R Proving Ground, cited 2013: The GOES-R Proving Ground at the Hazardous
11 Weather Testbed. [Available online at <http://goesrhwt.blogspot.com/>].

12 Greene, D. R., and R. A. Clark, 1972: Vertically integrated liquid water- a new analysis
13 tool. *Mon. Wea. Rev.*, **100**, 548-552.

14 Hartung D.C., J.M. Sieglaff, L.M. Cronic, and W.F. Feltz ,2013: An Inter-Comparison
15 of UW Cloud-Top Cooling Rates with WSR-88D Radar Data. *Wea. Forecasting*,
16 **28**, 463-480.

17 Heidinger, A.K., 2011: ABI Cloud Mask Algorithm Theoretical Basis Document.
18 NOAA NESDIS Center for Satellite Applications and Research (STAR), 67 pp.

19 Lakshmanan, V., A. Fritz, T. Smith, K. Hondl, and G. J. Stumpf, 2007: An automated
20 technique to quality control radar reflectivity data. *J. Appl. Meteor.*, **46**, 288-305.

21 -----, V., T. Smith, K. Hondl, G. J. Stumpf, and A. Witt, 2006: A real-time, three-
22 dimensional, rapidly updating, heterogeneous radar merger technique for

1 reflectivity, velocity and derived products. *Wea. Forecasting*, **21**, 802-823.

2 Mecikalski, J. R., P.D. Watts, and M. Koenig, 2011: Use of Meteosat Second Generation
3 optimal cloud analysis fields for understanding physical attributes of growing
4 cumulus clouds. *Atmos. Res.*, **102**, 175-190.

5 Mecikalski, J. R., and K. M. Bedka, 2006: Forecasting convective initiation by
6 monitoring the evolution of moving cumulus in daytime GOES imagery. *Mon.*
7 *Wea. Rev.*, **134**, 49-78.

8 Morel, C., and S. Senesi, 2002: A climatology of mesoscale convective systems over
9 Europe using satellite infrared imagery. I: Methodology. *Quart. J. Roy. Meteor.*
10 *Soc.*, **128**, 1953-1971.

11 Nakajima T. and M. D. King, 1990: Determination of Optical Thickness and Effective
12 Particle Radius of Cloud from Reflected Solar Radiation Measurements. Part I:
13 Theory. *J. Atmos. Sci.*, **47**, 1878-1893.

14 NEXRAD, 1985: Next generation weather radar (NEXRAD) algorithm report. NEXRAD
15 Joint System Program Office, Washington, DC.

16 Ortega, K. L., T. M. Smith, and G. J. Stumpf, 2006: Verification of multi-sensor, multi-
17 radar hail diagnosis techniques. Preprints, *Symposium on the Challenges of*
18 *Severe Convective Storms*, Atlanta, GA, Amer. Meteor. Soc. CD-ROM. P1.1

19 Pavolonis, M.J., 2010: ABI Cloud Type/Phase Algorithm Theoretical Basis Document.
20 NOAA NESDIS Center for Satellite Applications and Research (STAR), 60 pp.

21 Platnick, S. M.D. King, S.A. Ackerman, W.P. Menzel, B.A. Baum, J.C. Riedi, and R.A.
22 Frey, 2003: The MODIS Cloud Products: Algorithms and Examples From Terra.
23 *IEEE Trans. Geosci. Remote Sens.*, **41**, 459-473.

1 Roberts, R. D., and S. Rutledge, 2003: Nowcasting storm initiation and growth using
2 *GOES-8* and WSR-88D data. *Wea. Forecasting*, **18**, 562-584.

3 Schmit, T. J., M. M. Gunshor, W. P. Menzel, J. J. Gurka, J. Li, and A. S. Bachmeier,
4 2005: Introducing the next-generation Advanced Baseline Imager on goes-R.
5 *Bull. Am. Meteorol. Soc.*, **86**, doi:10.1175/BAMS-86-8-1079.

6 Sieglaff, J. M., D. C. Hartung, W. F. Feltz, L. M. Counce, and V. Lakshmanan, 2013:
7 Development and application of a satellite-based convective cloud object-tracking
8 methodology: A multipurpose data fusion tool. *J. Atmos. Oceanic Technol.*, **30**,
9 510-525.

10 Sieglaff, J. M., L. M. Counce, W. F. Feltz, K. M. Bedka, M. J. Pavolonis, and A. K.
11 Heidinger, 2011: Nowcasting convective storm initiation using satellite-based
12 box-averaged cloud-top cooling and cloud-type trends. *J. Atmos. Oceanic
13 Technol.*, **50**, 110-126.

14 Stumpf, G. J., T. M. Smith, and J. Hocker, 2004: New hail diagnostic parameters derived
15 by integrating multiple radars and multiple sensors. *22nd Conf. on Severe Local
16 Storms*, Amer. Meteor. Soc., Hyannis, MA, P7.8.

17 University of Wisconsin-Cooperative Institute for Meteorological Satellite Studies (UW-
18 CIMSS) cited 2013: Zoomerang Poll Results. [Available online at
19 http://cimss.ssec.wisc.edu/goes_r/proving-ground/SPC/UWCI_Feedback.html].

20 Vila, D. A., L. A. T. Machado, H. Laurent, and I. Velasco, 2008: Forecasting and
21 Tracking the Evolution of Cloud Clusters (ForTraCC) using satellite infrared
22 imagery: Methodology and validation. *Wea. Forecasting*, **23**, 233-245.

- 1 Walther, A. and A. Heidinger, 2012: Implementation of the Daytime Cloud Optical and
2 Microphysical Properties Algorithm (DCOMP) in PATMOS-X. *J. Appl. Meteor.*
3 *Climatol.*, **51**, 1371-1390.
- 4 Witt, A., M. D. Eilts, G. J. Stumpf, J. T. Johnson, E. D. W. Mitchell, and K. W. Thomas,
5 1998a: An enhanced hail detection algorithm for the WSR-88D. *Wea.*
6 *Forecasting*. **13**, 286-303.
- 7 Witt, A., M. D. Eilts, G. J. Stumpf, E. D. Mitchell, J. T. Johnson, and K. W. Thomas,
8 1998b: Evaluating the performance of WSR-88D severe storm detection
9 algorithms. *Weather and Forecasting*, **13**, doi:10.1175/
10 Zinner, T., H. Mannstein, and A. Tafferner, 2008: Cb-TRAM: Tracking and monitoring
11 severe convection from onset over rapid development to mature phase using
12 multi-channel *Meteosat-8* SEVIRI data. *Meteor. Atmos. Phys.*, **101**, 191-210.

1 Table 1: Hit, miss, false alarm, Probability of Detection (POD), False Alarm Ratio
2 (FAR), and Critical Success Index (CSI) statistics for CTC (v1 (non-bold) and v2 (bold))
3 and radar reflectivity threshold at the -10°C isotherm (Ref.₁₀) for the Interior Plains
4 region of the US for the 23 convective days within the validation dataset. Hit and miss
5 counts include all hits and misses for Ref.₁₀ greater than or equal to the bin value. False
6 alarm counts include cloud objects that had a CTC signal and no Ref.₁₀ value, as well as
7 those objects that had a cooling rate and achieved a maximum Ref.₁₀ less than the bin
8 value. A ‘hit’ is defined as any cloud object that was assigned a CTC rate and also
9 achieved a Ref.₁₀ value of the corresponding bin magnitude or greater during its lifetime.
10 A ‘miss’ is a cloud object that achieved a Ref.₁₀ magnitude that was greater than or equal
11 to the bin value during its lifetime but was never assigned a CTC rate, or any cloud object
12 that achieved a Ref.₁₀ magnitude greater than or equal to the corresponding bin *prior to* it
13 being assigned a corresponding CTC rate. The italicized POD, FAR, and CSI values are
14 for all CTC values without distinction for CTC magnitude.

15
16
17
18
19
20
21
22
23
24
25
26
27
28
29
30
31

	Weak [Ref-10 < 35 dBZ]		Moderate [35 dBZ ≤ Ref-10 < 60 dBZ]										Strong [Ref-10 ≥ 60 dBZ]	
Ref at - 10°C	< 35 dBZ		35 dBZ		40 dBZ		45 dBZ		50 dBZ		55 dBZ		≥ 60 dBZ	
Total Hits	302	260	225	194	190	169	160	138	128	108	93	78	55	45
Total Misses*	2851	2893	897	928	563	584	326	348	160	180	69	84	22	32
Total False Alarms	215	174	231	190	232	189	233	191	224	188	224	190	238	208
POD														
All CTC	0.10	<i>0.08</i>	0.20	<i>0.17</i>	0.25	<i>0.22</i>	0.33	<i>0.28</i>	0.44	<i>0.38</i>	0.57	<i>0.48</i>	0.71	<i>0.58</i>
> -10	0.02	0.03	0.03	0.05	0.03	0.06	0.04	0.07	0.04	0.09	0.04	0.09	0.03	0.08
-10 ≥ > -20	0.04	0.04	0.08	0.08	0.10	0.10	0.12	0.12	0.15	0.16	0.13	0.18	0.14	0.21
≤ -20	0.03	0.02	0.09	0.05	0.12	0.07	0.17	0.09	0.25	0.13	0.41	0.21	0.55	0.30
FAR														
All CTC	0.42	<i>0.40</i>	0.51	<i>0.49</i>	0.55	<i>0.53</i>	0.59	<i>0.58</i>	0.64	<i>0.64</i>	0.71	<i>0.71</i>	0.81	<i>0.82</i>
> -10	0.08	0.14	0.11	0.19	0.13	0.21	0.15	0.24	0.16	0.25	0.18	0.28	0.18	0.30
-10 ≥ > -20	0.19	0.16	0.23	0.20	0.25	0.22	0.27	0.23	0.28	0.26	0.31	0.29	0.34	0.34
≤ -20	0.14	0.09	0.16	0.11	0.17	0.10	0.18	0.11	0.20	0.13	0.22	0.14	0.29	0.17
CSI														
All CTC	0.09	<i>0.08</i>	0.17	<i>0.15</i>	0.19	<i>0.18</i>	0.22	<i>0.20</i>	0.25	<i>0.23</i>	0.24	<i>0.22</i>	0.17	<i>0.16</i>
> -10	0.02	0.03	0.04	0.05	0.04	0.06	0.05	0.08	0.05	0.09	0.05	0.09	0.03	0.05
-10 ≥ > -20	0.04	0.04	0.08	0.08	0.10	0.10	0.12	0.12	0.14	0.15	0.11	0.15	0.08	0.12
≤ -20	0.04	0.02	0.09	0.05	0.13	0.07	0.18	0.11	0.24	0.15	0.32	0.22	0.28	0.23

1

2

3

- 1 Table 2. Counts of cloud objects in the validation scheme with maximum observed CTC
- 2 and any measured value of the radar-derived fields broken down by CTC intensity for v1
- 3 (top) and v2 (bottom) in the validation domain.

Maximum CTC Rates Intensity [$K (15min)^{-1}$]	Ref-10	VIL	MESH
v1 > -10	83	32	18
-10 \geq v1 > -20	114	72	41
v1 \leq -20	63	48	37
v2 > -10	58	17	5
-10 \geq v2 > -20	135	85	32
v2 \leq -20	109	102	82

4

1 Table 3. Counts of cloud objects for all CTC and any measured value of the radar-
 2 derived fields broken down by CTC intensity for v1 (top) and v2 (bottom) in the
 3 validation domain. All CTC refers to all cooling rates exhibited by a single cloud object.
 4 For example, if a cloud object exhibited weak, moderate, and strong CTC at different
 5 times of growth, the cloud object would be counted in each CTC bin, as opposed to only
 6 the strong CTC bin in Table 2. As such, Table 3 has more counts than Table 2.

7

All CTC Rates Intensity [K (15min) ⁻¹]	Ref. ₁₀	VIL	MESH
v1 > -10	151	91	47
-10 ≥ v1 > -20	172	125	77
v1 ≤ -20	79	64	50
v2 > -10	159	107	59
-10 ≥ v2 > -20	259	191	115
v2 ≤ -20	164	156	128

8

1
2 Table 4: Hit, miss, false alarm, Probability of Detection (POD), False Alarm Ratio
3 (FAR), and Critical Success Index (CSI) statistics for CTC (v1 (non-bold) and v2 (bold))
4 and radar-estimated maximum expected size of hail (MESH) for the Interior Plains region
5 of the US for the 23 convective days within the validation dataset. Hit and miss counts
6 include all hits and misses for MESH greater than or equal to the bin value. False alarm
7 counts include cloud objects that had a CTC signal and no MESH value, as well as those
8 objects that had a cooling rate and achieved a maximum MESH less than the bin value. A
9 ‘hit’ is defined as any cloud object that was assigned a CTC rate and also achieved a
10 MESH value of the corresponding bin magnitude or greater during its lifetime. A ‘miss’
11 is a cloud object that achieved a MESH magnitude that was greater than or equal to the
12 bin value during its lifetime but was never assigned a CTC rate, or any cloud object that
13 achieved a MESH magnitude greater than or equal to the corresponding bin *prior to* it
14 being assigned a corresponding CTC rate. The italicized POD, FAR, and CSI values are
15 for all CTC values without distinction for CTC magnitude.

16
17
18
19
20
21
22
23
24

MESH (inches)	0.25		0.50		0.75		1.00		1.50		≥ 2.00	
Total Hits	119	96	103	80	77	62	62	50	40	32	25	20
Total Misses*	68	91	51	80	23	38	13	25	4	12	2	7
Total False Alarms	203	178	211	184	222	196	227	200	246	215	262	227
POD												
All CTC	0.64	<i>0.51</i>	0.67	<i>0.52</i>	0.77	<i>0.62</i>	0.83	<i>0.67</i>	0.91	<i>0.73</i>	0.93	<i>0.74</i>
> -10	0.03	0.09	0.03	0.09	0.02	0.11	0.01	0.09	0.00	0.09	0.00	0.07
-10 ≥ > -20	0.17	0.21	0.16	0.21	0.12	0.23	0.15	0.24	0.14	0.27	0.19	0.30
≤ -20	0.44	0.21	0.48	0.21	0.63	0.28	0.67	0.33	0.77	0.36	0.74	0.37
FAR												
All CTC	0.63	<i>0.65</i>	0.67	<i>0.70</i>	0.74	<i>0.76</i>	0.79	<i>0.80</i>	0.86	<i>0.87</i>	0.91	<i>0.92</i>
> -10	0.17	0.27	0.17	0.27	0.18	0.28	0.19	0.30	0.19	0.31	0.19	0.32
-10 ≥ > -20	0.29	0.26	0.30	0.29	0.33	0.32	0.34	0.34	0.35	0.36	0.36	0.38
≤ -20	0.17	0.12	0.20	0.14	0.23	0.16	0.26	0.16	0.32	0.20	0.37	0.22
CSI												
All CTC	0.31	0.26	0.28	<i>0.24</i>	0.24	<i>0.21</i>	0.21	<i>0.18</i>	0.14	<i>0.12</i>	0.09	<i>0.08</i>
> -10	0.04	0.10	0.05	0.09	0.03	0.09	0.01	0.07	0.00	0.04	0.00	0.02
-10 ≥ > -20	0.17	0.20	0.14	0.18	0.09	0.16	0.09	0.14	0.05	0.11	0.05	0.07
≤ -20	0.40	0.23	0.40	0.23	0.41	0.26	0.36	0.28	0.26	0.21	0.16	0.14

1

2

1 Table 5: Hit, miss, false alarm, Probability of Detection (POD), False Alarm Ratio
2 (FAR), and Critical Success Index (CSI) statistics for CTC (v1 (non-bold) and v2 (bold))
3 and radar vertically integrated liquid (VIL) for the Interior Plains region of the US for the
4 23 convective days within the validation dataset. Hit and miss counts include all hits and
5 misses for VIL greater than or equal to the bin value. False alarm counts include cloud
6 objects that had a CTC signal and no VIL value, as well as those objects that had a
7 cooling rate and achieved a maximum VIL less than the bin value. A ‘hit’ is defined as
8 any cloud object that was assigned a CTC rate and also achieved a VIL value of the
9 corresponding bin magnitude or greater during its lifetime. A ‘miss’ is a cloud object that
10 achieved a VIL magnitude that was greater than or equal to the bin value during its
11 lifetime but was never assigned a CTC rate, or any cloud object that achieved a VIL
12 magnitude greater than or equal to the corresponding bin *prior to* it being assigned a
13 corresponding CTC rate. The italicized POD, FAR, and CSI values are for all CTC
14 values without distinction for CTC magnitude.

15
16
17
18
19
20
21
22
23

VIL (kg m ⁻²)	5		10		20		30		40		≥ 50	
Total Hits	204	158	169	128	121	96	84	66	63	48	40	35
Total Misses*	287	333	191	232	87	112	32	50	23	28	5	10
Total False Alarms	202	183	202	183	213	186	216	192	226	202	246	212
POD												
All CTC	0.42	0.32	0.47	0.36	0.58	0.46	0.72	0.57	0.83	0.63	0.89	0.78
> -10	0.03	0.08	0.04	0.09	0.03	0.10	0.03	0.10	0.01	0.09	0.00	0.07
-10 ≥ > -20	0.17	0.15	0.17	0.15	0.17	0.18	0.14	0.22	0.13	0.22	0.11	0.31
≤ -20	0.21	0.10	0.26	0.11	0.38	0.18	0.56	0.25	0.68	0.32	0.78	0.40
FAR												
All CTC	0.50	0.54	0.54	0.59	0.64	0.66	0.72	0.74	0.78	0.81	0.86	0.86
> -10	0.15	0.23	0.16	0.24	0.17	0.27	0.18	0.28	0.19	0.30	0.19	0.31
-10 ≥ > -20	0.21	0.21	0.24	0.23	0.28	0.26	0.32	0.31	0.34	0.34	0.36	0.36
≤ -20	0.14	0.10	0.15	0.12	0.19	0.13	0.22	0.15	0.25	0.16	0.31	0.19
CSI												
All CTC	0.29	0.23	0.30	0.24	0.29	0.24	0.25	0.21	0.21	0.17	0.14	0.14
> -10	0.05	0.08	0.05	0.09	0.04	0.10	0.03	0.09	0.01	0.06	0.00	0.03
-10 ≥ > -20	0.19	0.15	0.18	0.15	0.16	0.17	0.11	0.16	0.08	0.13	0.04	0.13
≤ -20	0.23	0.12	0.28	0.13	0.35	0.20	0.40	0.25	0.38	0.26	0.27	0.24

1

2

1 Table 6: Median lead-time [min] of maximum CTC hits v2 (left) and v1 (right) versus for
 2 various thresholds of Ref.₁₀, MESH, and VIL (Tables 1, 4, and 5, respectively) for storms
 3 during the 23 convective afternoons studied. The lead-time analysis was bounded by a
 4 maximum lead-time of 60 minutes; hence the use of 60+ in these situations to reflect the
 5 actual lead-time may have exceeded 60 minutes.

NEXRAD Field		v2	v1
Ref.₁₀ [dBZ]	35	13	21
	45	20	26
	50	25	32
	55	31	39
	60	41	49
	65	60+	60+
MESH [in]	0.25"	28	36
	0.50"	33	41
	0.75"	38	58
	1.00"	51	60+
	1.50"	60+	60+
VIL [kg m⁻²]	10	23	32
	20	26	36
	30	33	46
	40	44	60+
	50	55	60+

6

1 **Figure Captions**

2 Figure 1. GOES visible (first (left) column), GOES 10.7 μm IRW BT (second column),
3 GOES visible optical depth retrieval (third column), and CTC algorithm ice mask (fourth
4 (right) column) on 30 March 2012 (valid times indicated on figure) over eastern Illinois
5 and western Indiana. A line of developing thunderstorms is evident in the visible and
6 IRW imagery. The increasing visible reflectances and cooling IRW BTs associated with
7 developing thunderstorms are co-located in space and time with increasing retrieved
8 visible optical depth. The ice mask regions are where v1 would not diagnose cloud-top
9 cooling rates.

10

11 Figure 2. GOES visible (first (left) column), GOES visible optical depth retrieval
12 (second column), v1 CTC rates (third column), v2 CTC rates (fourth column), and CTC
13 algorithm ice mask (fifth (right) column) on 30 March 2012 (valid times indicated on
14 figure) over eastern Illinois and western Indiana. V2 detects more developing
15 thunderstorms than v1.

16

1 Figure 3. GOES visible (first (left) column), GOES visible optical depth retrieval
2 (second column), v1 CTC rates (third column), v2 CTC rates (fourth column), and CTC
3 algorithm ice mask (fifth (right) column) on 14 April 2011 (valid times indicated on
4 figure) over Oklahoma. V2 detects more developing thunderstorms than v1 (northern
5 Oklahoma) as well as the most intense period of cooling in the southern storm at 2003
6 UTC.

7
8 Figure 4. Comparison of all instantaneous (top) and maximum (bottom) CTC for v2
9 (left) and v1 (right) to maximum reflectivity at -10°C isotherm [Ref_{-10} ; dBZ] for cloud-
10 objects that had both a CTC and associated Ref_{-10} at some point in their lifetime. CTC
11 rates for cloud-objects are binned by intensity [K (15 min)^{-1}] with weak, moderate, and
12 strong convective growth defined as $\text{CTC} > -10$, $-10 \geq \text{CTC} > -20$, and $\text{CTC} \leq -20$,
13 respectively. For each boxplot, the median (red line), 25th and 75th percentiles (lower and
14 upper bounds of blue box), and one standard deviation (whiskers) are shown. The
15 medians of different intensity bins are significantly different at the 5% significance level
16 if the widths of the notches centered on the medians do not overlap.

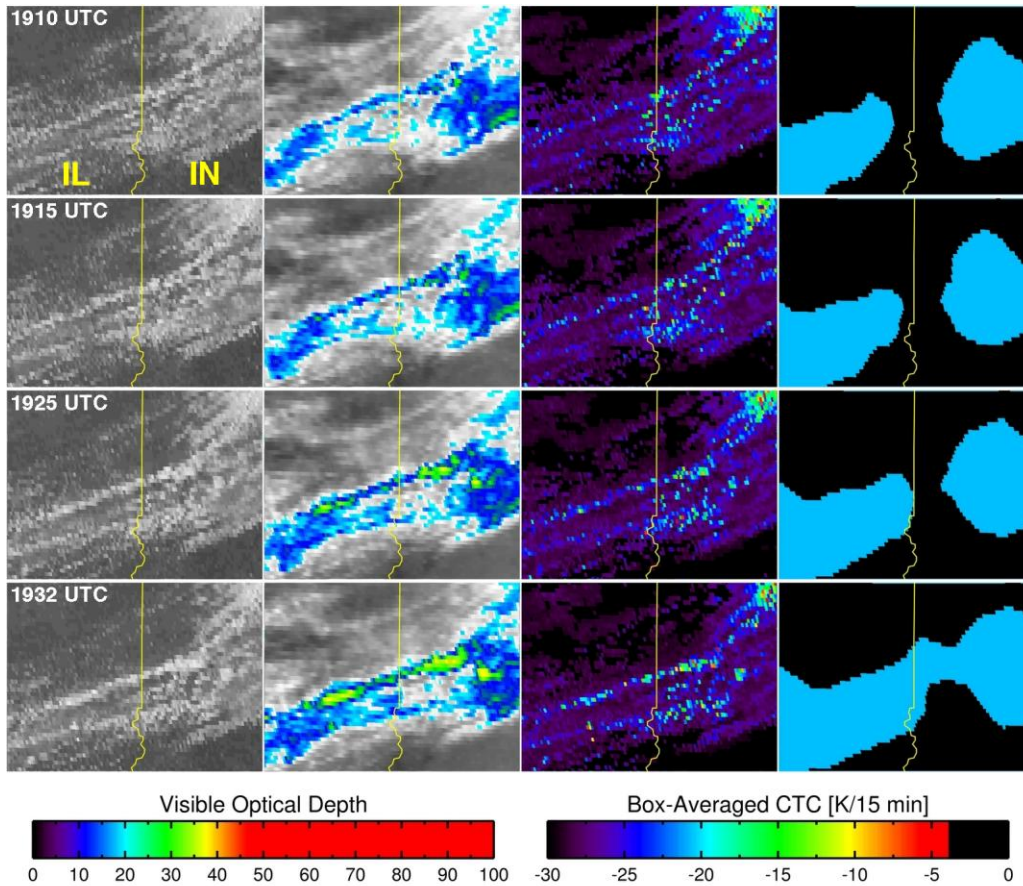
17
18 Figure 5. Comparison of all instantaneous (top) and maximum (bottom) CTC for v2
19 (left) and v1 (right) to Maximum Estimated Size of Hail [MESH; in] for cloud-objects
20 that had both a CTC and associated MESH at some point in their lifetime. CTC rates for
21 cloud-objects are binned by intensity [K (15 min)^{-1}] with weak, moderate, and strong
22 convective growth defined as $\text{CTC} > -10$, $-10 \geq \text{CTC} > -20$, and $\text{CTC} \leq -20$, respectively.
23 For each boxplot, the median (red line), 25th and 75th percentiles (lower and upper bounds

1 of blue box), and one standard deviation (whiskers) are shown. The medians of different
2 intensity bins are significantly different at the 5% significance level if the widths of the
3 notches centered on the medians do not overlap.

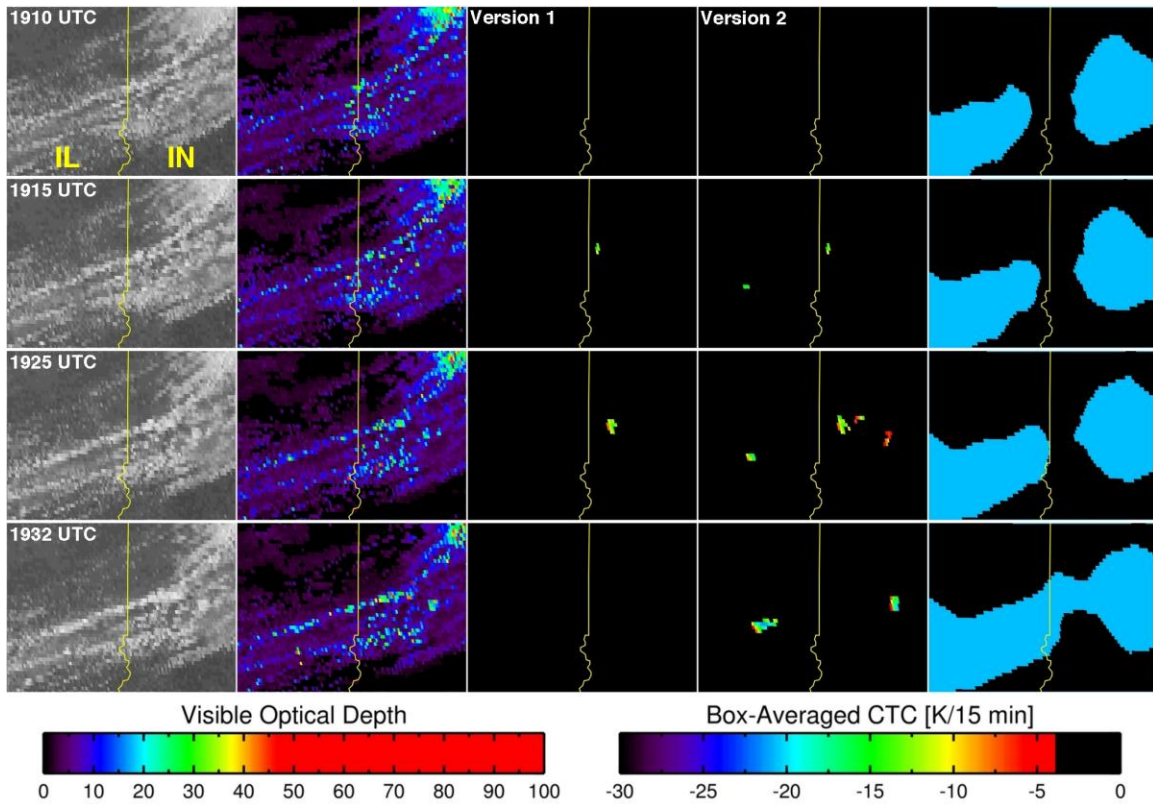
4

5 Figure 6. Comparison of all instantaneous (top) and maximum (bottom) CTC for v2
6 (left) and v1 (right) to Vertically Integrated Liquid [VIL; kg m^{-2}] for cloud-objects that
7 had both a CTC and associated VIL at some point in their lifetime. CTC rates for cloud-
8 objects are binned by intensity [K (15 min)^{-1}] with weak, moderate, and strong
9 convective growth defined as $\text{CTC} > -10$, $-10 \geq \text{CTC} > -20$, and $\text{CTC} \leq -20$, respectively.
10 For each boxplot, the median (red line), 25th and 75th percentiles (lower and upper bounds
11 of blue box), and one standard deviation (whiskers) are shown. The medians of different
12 intensity bins are significantly different at the 5% significance level if the widths of the
13 notches centered on the medians do not overlap.

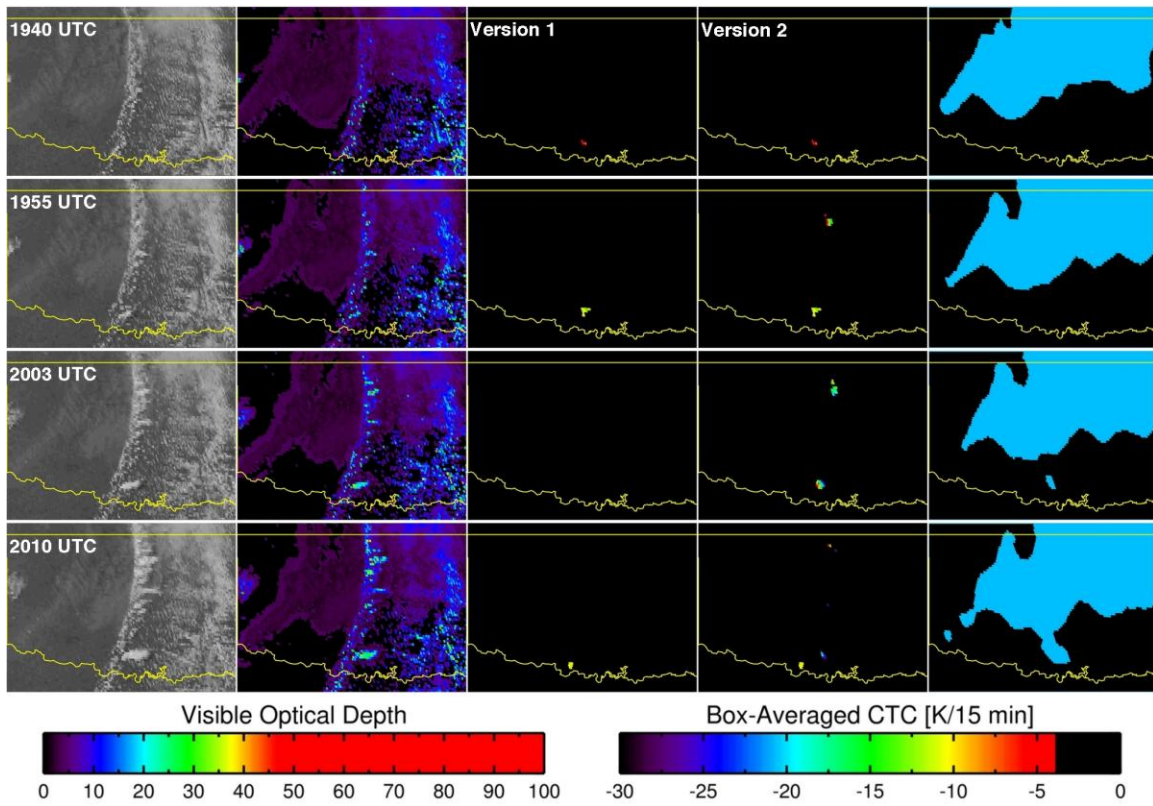
14



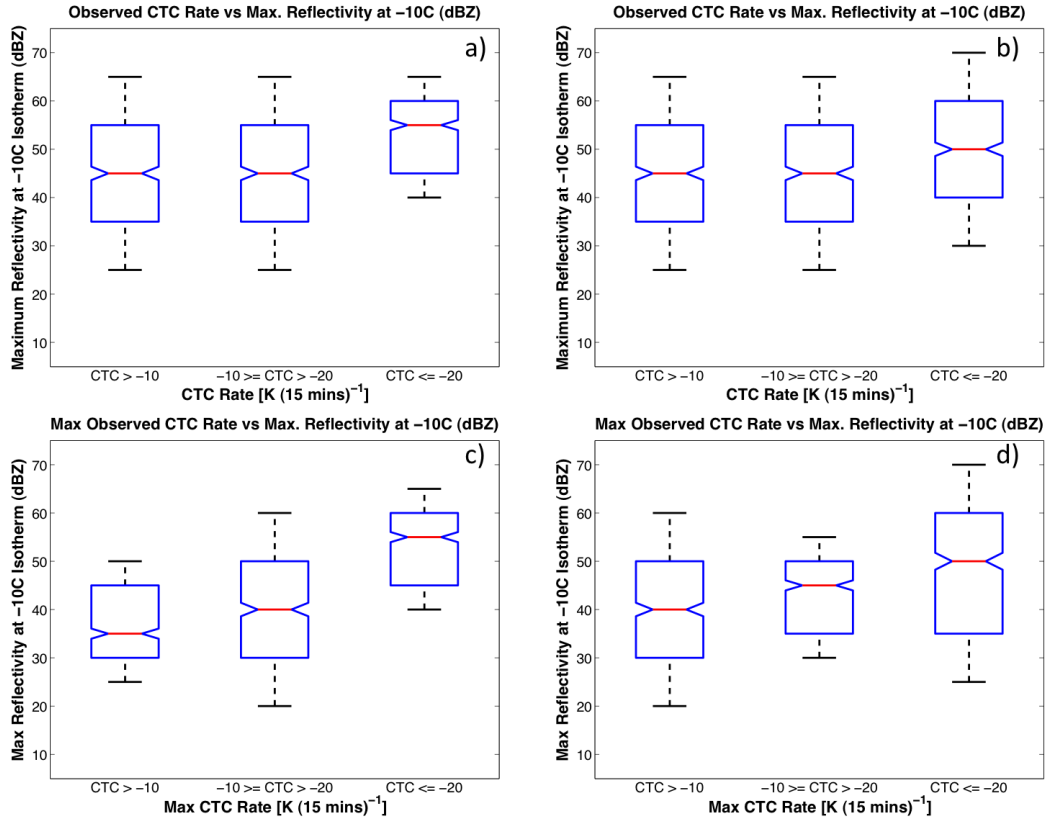
1
 2 Figure 1. GOES visible (first (left) column), GOES 10.7 μm IRW BT (second column),
 3 GOES visible optical depth retrieval (third column), and CTC algorithm ice mask (fourth
 4 (right) column) on 30 March 2012 (valid times indicated on figure) over eastern Illinois
 5 and western Indiana. A line of developing thunderstorms is evident in the visible and
 6 IRW imagery. The increasing visible reflectances and cooling IRW BTs associated with
 7 developing thunderstorms are co-located in space and time with increasing retrieved
 8 visible optical depth. The ice mask regions are where v1 would not diagnose cloud-top
 9 cooling rates.



1
 2 Figure 2. GOES visible (first (left) column), GOES visible optical depth retrieval
 3 (second column), v1 CTC rates (third column), v2 CTC rates (fourth column), and CTC
 4 algorithm ice mask (fifth (right) column) on 30 March 2012 (valid times indicated on
 5 figure) over eastern Illinois and western Indiana. V2 detects more developing
 6 thunderstorms than v1.
 7

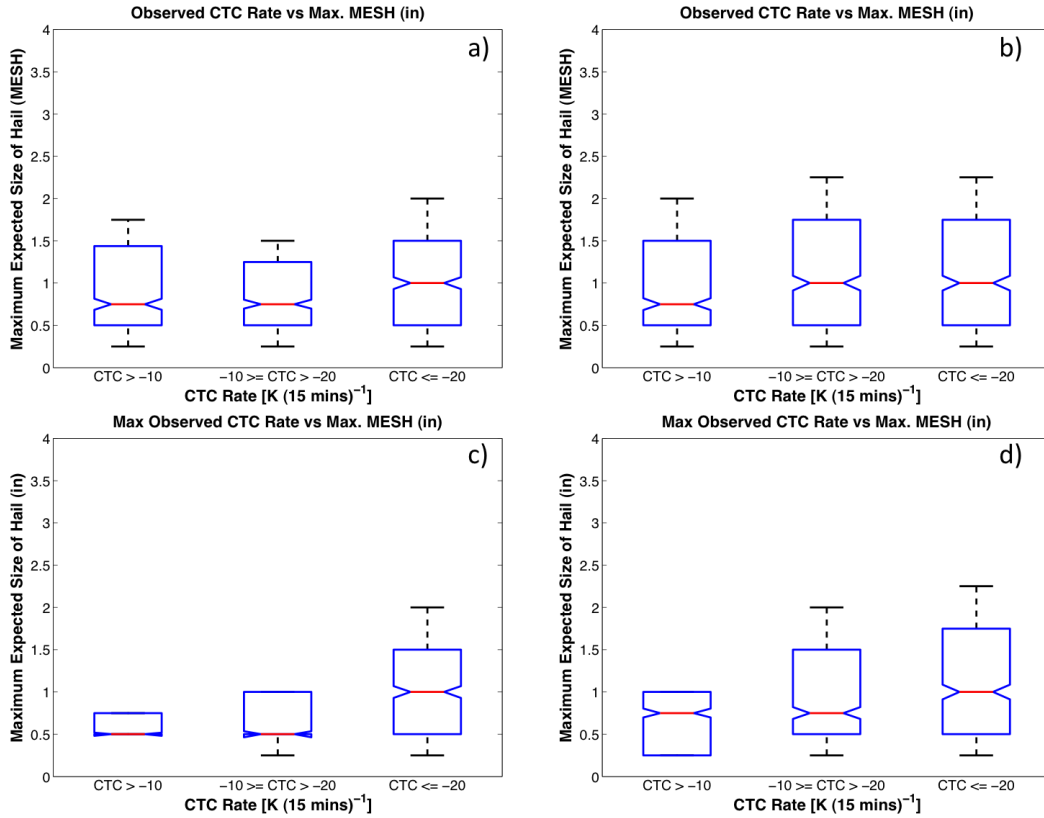


1
 2 Figure 3. GOES visible (first (left) column), GOES visible optical depth retrieval
 3 (second column), v1 CTC rates (third column), v2 CTC rates (fourth column), and CTC
 4 algorithm ice mask (fifth (right) column) on 14 April 2011 (valid times indicated on
 5 figure) over Oklahoma. V2 detects more developing thunderstorms than v1 (northern
 6 Oklahoma) as well as the most intense period of cooling in the southern storm at 2003
 7 UTC.

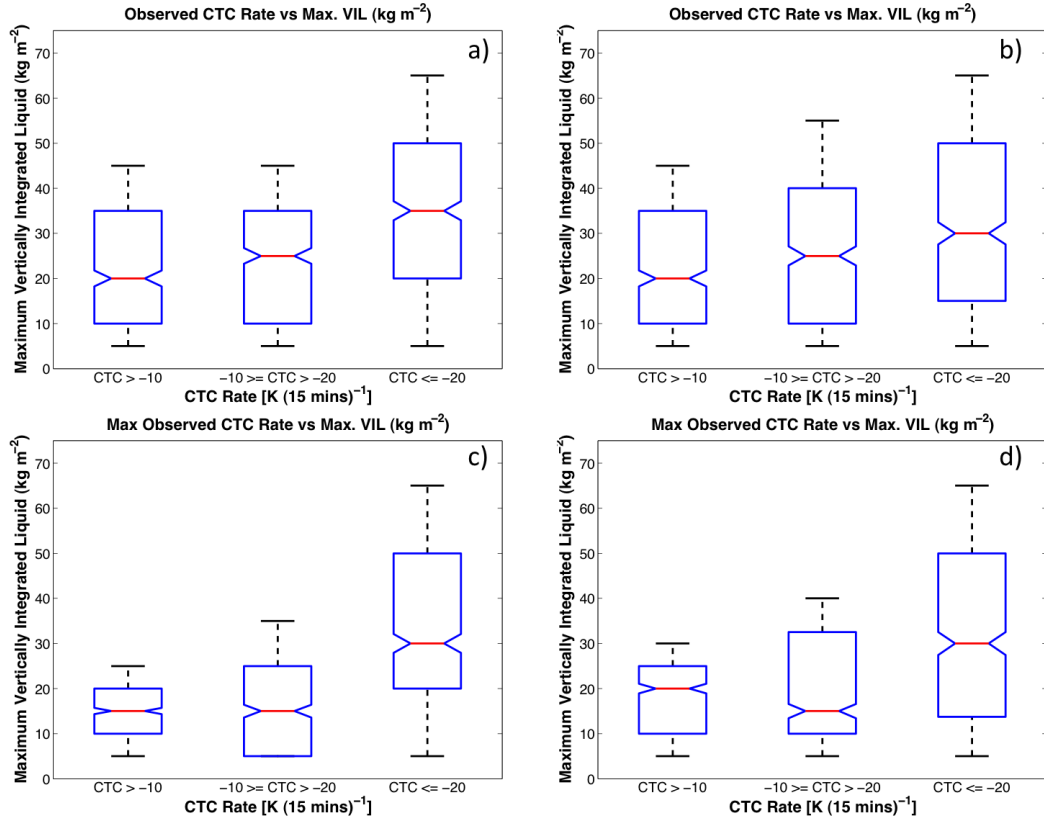


1
2
3
4
5
6
7
8
9
10
11

Figure 4. Comparison of all instantaneous (top) and maximum (bottom) CTC for v2 (left) and v1 (right) to maximum reflectivity at -10°C isotherm [Ref_{10} ; dBZ] for cloud-objects that had both a CTC and associated Ref_{10} at some point in their lifetime. CTC rates for cloud-objects are binned by intensity [K (15 min)^{-1}] with weak, moderate, and strong convective growth defined as $\text{CTC} > -10$, $-10 \geq \text{CTC} > -20$, and $\text{CTC} \leq -20$, respectively. For each boxplot, the median (red line), 25th and 75th percentiles (lower and upper bounds of blue box), and one standard deviation (whiskers) are shown. The medians of different intensity bins are significantly different at the 5% significance level if the widths of the notches centered on the medians do not overlap.



1
 2 Figure 5. Comparison of all instantaneous (top) and maximum (bottom) CTC for v2
 3 (left) and v1 (right) to Maximum Estimated Size of Hail [MESH; in] for cloud-objects
 4 that had both a CTC and associated MESH at some point in their lifetime. CTC rates for
 5 cloud-objects are binned by intensity $[K (15 \text{ mins})^{-1}]$ with weak, moderate, and strong
 6 convective growth defined as $CTC > -10$, $-10 \geq CTC > -20$, and $CTC \leq -20$, respectively.
 7 For each boxplot, the median (red line), 25th and 75th percentiles (lower and upper bounds
 8 of blue box), and one standard deviation (whiskers) are shown. The medians of different
 9 intensity bins are significantly different at the 5% significance level if the widths of the
 10 notches centered on the medians do not overlap.



1

2 Figure 6. Comparison of all instantaneous (top) and maximum (bottom) CTC for v2
 3 (left) and v1 (right) to Vertically Integrated Liquid [VIL; kg m^{-2}] for cloud-objects that
 4 had both a CTC and associated VIL at some point in their lifetime. CTC rates for cloud-
 5 objects are binned by intensity [K (15 min)^{-1}] with weak, moderate, and strong
 6 convective growth defined as $\text{CTC} > -10$, $-10 \geq \text{CTC} > -20$, and $\text{CTC} \leq -20$, respectively.
 7 For each boxplot, the median (red line), 25th and 75th percentiles (lower and upper bounds
 8 of blue box), and one standard deviation (whiskers) are shown. The medians of different
 9 intensity bins are significantly different at the 5% significance level if the widths of the
 10 notches centered on the medians do not overlap.